

Incorporating new functions into the WAVES model, to better simulate cotton production under film mulching and severe salinity

Qihua Yu ^{a,b}, Shaozhong Kang ^{a,b,*}, Lu Zhang ^{c,d}, Shunjun Hu ^e, Yunfeng Li ^f, David Parsons ^g

^a Center for Agricultural Water Research in China, China Agricultural University, Beijing 100083, China

^b National Field Scientific Observation and Research Station on Efficient Water Use of Oasis Agriculture, Wuwei 733009, China

^c State Key Laboratory of Water Resources Engineering and Management, Wuhan University, Wuhan 430072, China

^d CSIRO Land and Water, Black Mountain, Canberra, ACT 2601, Australia

^e State Key Laboratory of Desert and Oasis Ecology, Xinjiang Institute of Ecology and Geography, Chinese Academy of Science (CAS), Urumqi 830011, China

^f Key Open Laboratory of Crop Water Requirement and Regulation, Institute of Farmland Irrigation, Chinese Academy of Agricultural Sciences, Ministry of Agriculture and Rural Affairs, Xinxiang 453002, China

^g Department of Crop Production Ecology, Swedish University of Agricultural Sciences, Umeå 90183, Sweden

ARTICLE INFO

Handling Editor: Dr Z Xiyang

Keywords:

Film mulching
Modeling
Evaporation
Soil water
WAVES model

ABSTRACT

Film mulching is widely used as an agronomic practice to counteract water scarcity in arid and semi-arid areas. Although crop models have emerged as powerful tools for system studies and scenarios analysis, they have been rarely used in areas with severe drought and salinization and where mulching is being used as a management practice. An earlier study shown great modelling potential under severe salinity in southern Xinjiang, China. The model is WAVES (the WATER Vegetation Energy and Solute), while evaporation was overestimated in the earlier study without considering the mulching effect. In this study, we used a modified WAVES model by incorporating three functions working on potential evaporation, underlying surface albedo, and soil resistance into it to represent the mulching effect. Calibration and validation were conducted using cotton field experiments from 2 different years. Of the 3 functions evaluated, the one representing potential evaporation reduction exerted the highest modification effect on soil water status. The modified model better simulated evaporation, soil-water content, soil-salt content, leaf area index (LAI), and yield than the original model, decreasing normalized root mean square error (NRMSE) by 173%, 15%, 14%, 9%, and 35%, respectively. The modification effects were most significant during the seedling stage. In addition, the modified model produced a higher realistic evaporation (E)/evapotranspiration (ET) under the film mulching environment. These findings suggest that the modified WAVES model can be applied for crop management under film mulching, particularly in areas with low rainfall and high salinization.

1. Introduction

Water scarcity has been one of the major limitations to the production of crops in arid and semi-arid regions globally (Caparas et al., 2021; Elliott et al., 2014; Sun et al., 2018). Thus, water management is highly crucial to ensure increased and constant production of food for the world's growing population (Kang et al., 2017). Film mulching is a process that involves covering the crop areas with a film to protect them from adverse environmental conditions and preserve moisture, thereby recycling the lost water back into the soil. It was introduced in the 1950s and since then has been applied to overcome agricultural problems related to water shortage (Griffin-LaHue et al., 2022). The global use of

agricultural plastic films is projected to increase by 59% from 2018 to 2026 (Sintim et al., 2020). In northwest China, where agriculture heavily relies on irrigation, film mulching is increasingly being used to conserve water. For example, 64% of the cotton planting area in Xinjiang, China, is under film mulching, with a total area of 1.6 million hectares in 2021.

The effects of plastic film mulching on crop cultivation have been well documented by previous studies. The film functions by altering the growing environmental conditions, including increasing the underlying surface albedo, attenuating incident solar radiation, enhancing water vapor transfer resistance, reducing soil water evaporation, entrapping rainfall, and increasing soil temperature (Kader et al., 2017; Lisson et al.,

* Corresponding author at: Center for Agricultural Water Research in China, China Agricultural University, Beijing 100083, China.

E-mail address: kangsz@cau.edu.cn (S. Kang).

<https://doi.org/10.1016/j.agwat.2023.108470>

Received 1 February 2023; Received in revised form 1 August 2023; Accepted 2 August 2023

Available online 12 August 2023

0378-3774/© 2023 The Authors. Published by Elsevier B.V. This is an open access article under the CC BY-NC-ND license (<http://creativecommons.org/licenses/by-nc-nd/4.0/>).

2016; Wang et al., 2019; Xu et al., 2023). The changed growing environment consequently affects crop growth, for example, in terms of improved water use efficiency and increased crop yield (Gao et al., 2019; Lv et al., 2023; Zhao et al., 2020). However, the soil-plant-atmosphere continuum during mulching has not been studied much. A review by Kader et al. (2017) states a lack of process-based investigations on the effects of mulching. Crop models are useful and efficient tools that are process-based and reflect the crop responses to agronomic practices, and can contribute to the development of sustainable plans and management of crop production. It is possible to evaluate the impact of film mulching on underground soil status and aboveground crop growth using crop models.

Certain models have already added functions to study mulching effects. Models have been modified to accurately estimate single variables, such as evapotranspiration under mulching. For instance, Li et al. (2013) modified the Shuttleworth-Wallace (SW) model by considering the mulching effect on soil evaporation. Shukla et al. (2014) developed a crop coefficient for drip-irrigated watermelons grown with plastic mulch. Ding et al. (2015) modified the Penman-Monteith (PM) model by revising the surface resistance and assuming no evaporation in the film-covered area. In addition, certain complex systematic models have been studied under mulching. For example, the Hydrus-2D model considers the boundary condition of the crop area under the mulch as a no-flux boundary (He et al., 2018; Saglam et al., 2017). Moreover, other researchers considered the evaporation under the film as zero and calculated the reduction in soil evaporation by multiplying the potential evaporation and film cover fraction, for example in DNDC (Han et al., 2014), WHCNS (Liang et al., 2017), Hybrid-Maize model (Hou et al., 2014), and DSSAT-CERES (Shen et al., 2021). Other approaches include adding a newly developed surface albedo function with a mulching effect into the land surface model Two-Big-Leaf-SHAW (TBLSHAW) developed by Yang et al. (2012); another example is directly adjusting meteorological input data of rainfall when using the LandscapeDNDC model developed by Kim et al. (2014).

Researchers believe that the functions of models under mulching need to be strengthened. Although plastic film degrades slowly under environmental conditions, it could be broken on exposure to extreme weather events such as hail and storms due to physical fragmentation and chemical aging (Steinmetz et al., 2016). In addition, agronomic activities such as cotton top-cutting manually destroy the film, thereby greatly reducing the water-retention performance. However, studies on the effects of disintegrated areas of plastic film on soil water movement are limited. Besides, the mulching effects are variable for different environments and crops (Hou et al., 2014) because of the complex changes in the microenvironment and soil. Gao et al. (2019) reviewed the literatures and concluded that the effect of film mulching on crop yield was highest for potato, followed by cotton, wheat and maize. For the different regions, the highest yield increase was found in Central China, followed by Northwest China, Eastern China, North China and Northeast China. Thus, existing general models need to be modified to adapt them to specific natural conditions or agricultural settings for a more reliable estimation (Ai and Yang, 2016).

A few crop models have been used for mulched crops in areas of severe drought and high salinization (soil salt content greater than 6 g kg⁻¹, Gao et al., 2011). A review of the handful of studies on the subject has found that the results were underperforming (Qureshi et al., 2013; Su et al., 2005). Among the few studies available, a process-based model of WAVES stood out and was calibrated and applied to the crops grown in Southern Xinjiang, China, an area with water and salt stress (Yu et al., 2021). WAVES uses a possible and valuable expression (Integrated Rate Method, Wu et al., 1994) that shown modelling potential under high salinity. Yu et al. (2021) found WAVES could model dynamic changes of soil water and salt with high accuracy, while its inability to account for film mulching effect was also found. The WAVES model overestimated the growing season evaporation. This could potentially be improved by incorporating the film mulching effect. Thus, in the present study, we

modified the WAVES model by applying different functions from the above reviewed aspects and also considering dynamic film mulch cover fraction. The main purpose of this study is to incorporate the film mulching effect on water movement in WAVES model and evaluate the modification performance compared to the original WAVES model for cotton crop in Southern Xinjiang, China.

2. Materials and methods

2.1. Field experiments and measurements

2.1.1. Experiment A

Field experiment A was performed in 2021 at the Soil and Water Conservation Monitoring Station (E 81°12', N 40°37') of the First Division of Xinjiang Production and Construction Corps, China. The site is in a warm temperate zone with an arid climate. The annual average temperature, precipitation, relative humidity, sunshine hours, pan evaporation, and solar radiation are 11.3 °C, 45.7 mm, 48%, 2948 h, 2500 mm, and 6000 MJ m⁻², respectively.

We used the *Gossypium hirsutum* L. cv. Zhongmian 40 cotton variety. Four treatments (T1, T2, T3, and T4) were applied using different total irrigation amounts of 255, 330, 405, and 480 mm, respectively, with three replicates. Detailed irrigation schedule information is listed in Table S1. A transparent plastic film was used with drip irrigation. The irrigation water was obtained from a well and the water salinity was 2.18 g L⁻¹. The soil texture is sandy loam (64.2% sand, 34.1% silt, and 1.8% clay) with a bulk density of 1.60 g cm⁻³. The groundwater depth was deeper than 3 m during the whole growth period. The sowing was performed on April 14 and the harvesting was conducted on October 10. Crop management was performed according to local practices.

Meteorological data, including precipitation, temperature, sunshine hours, and solar radiation, were collected using an automatic weather station (HOBO, USA) at the experimental site. Rainfall and temperature values are shown in Fig. S1. Rainfall during the growing season was 64 mm in 2021. Soil samples were collected after harvest to determine the soil density, soil texture, and the characteristic curves of soil moisture. In addition, we collected soil samples during the growing season at depths of 0–10, 10–20, 20–30, 30–40, 40–60, and 60–80 cm to assess the soil water content (the gravimetric method) and soil salt content. The soil salt content was measured using an indirect method by determining the soil water electrical conductivity (EC_{1:5}, dS m⁻¹), which was measured on 1:5 extracts for soil and water (by weight). The soil salt content (SSC, g kg⁻¹) was empirically related to EC_{1:5} (Hu et al., 2013), as follows:

$$SSC = EC_{1:5} \times 4.61, (R^2 = 0.96; 517 \text{ soil samples}) \quad (1)$$

Daily soil evaporation was monitored using micro-lysimeters composed of polyvinyl chloride (PVC) tubes with a 10 cm inside diameter, installed at a depth of 20 cm. Soil evaporation was only measured in one treatment. Two replicates were installed in bare soil and daily evaporation was obtained by weighing micro-lysimeters using an electronic scale with a precision of 0.1 g at 21:00 Beijing time from July 26 to September 12 in 2021. On a rainy day, micro-lysimeters were reinstalled to minimize the difference between soil moisture inside and outside the tubes. The final measured soil evaporation was obtained by integrating the film cover fraction and the measured value from micro-lysimeters, assuming that the soil evaporation under the film area was zero. The calculation was as follows:

$$E_{est} = (1 - f_m)E_{mea} \quad (2)$$

where E_{est} is the estimated soil evaporation (mm d⁻¹) of the film mulching treatment, f_m is the film-covering fraction, and E_{mea} is the measured evaporation (mm d⁻¹) using micro-lysimeters. The film-covering fraction before sowing was 71%. Holes (about 3 cm in diameter) were created during sowing to enable the plants to grow above the film; thus, an f_m of 65% was used in this study for the 2021 experiment.

Next, the leaf area index (LAI) was estimated by measuring the length and maximum width of fully unfolded leaves from three representative cotton plants. Cotton yield (lint) for each treatment was measured at harvest by hand harvesting with replications in three plots, each plot measuring 2.28 m × 2.92 m.

2.1.2. Experiment B

Field experiment B was conducted in 2010 at the Aksu National Field Research Station of Agro-ecosystems (E 80°51', N 40°37'), Xinjiang Uygur Autonomous Region (Xinjiang), China. The two stations are within the same irrigation district and have the same climatic conditions and cotton growth stage durations.

We used the *Gossypium hirsutum* L. cv. Tuonong 1 variety of cotton. Four irrigation treatments (T1, T2, T3, and T4) were administered using different total irrigation amounts of 262.5, 375, 487.5, and 600 mm, respectively. Twelve irrigation events were conducted and detailed dates and irrigation amounts are listed in Table S2. A transparent film was used with drip irrigation, the same as in experiment A. Fresh water (surface water) with a low salinity concentration of 0.49 g L⁻¹ was used for irrigation. The soil texture was silty loam (25.4% sand, 69.4% silt, and 5.3% clay) with a bulk density of 1.48 g cm⁻³. The groundwater depth was generally around 2 m during the whole growth period. The sowing was performed on April 30, and the crop was harvested on November 4. Crop management was performed according to local practices.

An automatic weather station (HOBO, USA) was located at the experiment site. The maximum temperature, minimum temperature, and rainfall are shown in Fig. S2. The rainfall during the growing season was 65.7 mm in 2010, similar to that for experiment A. Soil samples were collected during the growing season to determine the soil density, texture, saturated hydraulic conductivity, and soil moisture characteristic curve. The soil water content was measured every 5 days using a neutron probe at depths of 10, 30, 50, and 70 cm. The neutron probe was calibrated by measuring the soil water content using the gravimetric method. To measure the soil salt content, soil samples were collected during the growing season at depths of 0–10, 10–20, 20–30, 30–40, 40–60, and 60–80 cm. The methods to obtain the soil salt content and soil evaporation (three replicates) were the same as those used in experiment A. The initial film cover fraction was 68%. Considering the opening holes (about 3 cm in diameter) for plants, an f_m of 60% was used in this study for the 2010 experiment. Cotton yield (lint) for each plot was measured at harvest by hand harvesting with three replicates.

2.2. Description of the WAVES model

WAVES (the WATER Vegetation Energy and Solute model), coded in FORTRAN, was developed by the Commonwealth Scientific and Industrial Research Organization in Australia (Zhang and Dawes, 1998). WAVES is a process-based model at a daily time-step, with a good balance between complexity, usefulness, and accuracy. WAVES can well predict the soil water budgets and evapotranspiration (ET) (Cheng et al., 2014; Gharun et al., 2018; Tian et al., 2017), crop growth and yield (Kang et al., 2003; Wang et al., 2001), groundwater recharge (Barron et al., 2012; Crosbie et al., 2013; Silberstein et al., 2013), and water and carbon balance (Gharun et al., 2018; Silberstein et al., 2013). In addition, WAVES solves Richard's equation and the convection dispersion equation to obtain soil water movement and solute transport through the soil profile. The model partitions the available energy into canopy and soil for plant growth and evapotranspiration, calculates carbon assimilation, and dynamically allocates carbon to leaves, stems, and roots. The model is described in details in the user manual (Zhang and Dawes, 1998). In addition, the model has been validated in Xinjiang (severe salinity) in a former study (Yu et al., 2021). Mulching is widely used in Xinjiang, China, and its impact on soil water status can't be ignored. The principle of WAVES model did not consider the mulching effect. Yu et al. (2021)'s study set the Kc (hydraulic conductivity) at a

very low value as 0.001 m day⁻¹ in the surface layer (0–0.002 m) to indirectly reflect the partial mulching effect. The modelling performance were good in Yu et al. (2021)'s study, while the soil water content in the earlier stage was underestimated and the evaporation was overestimated, indicating that WAVES model needs modification on mulching effect from a mechanistic perspective.

2.3. Modifications of the WAVES model

2.3.1. Function 1 reduction of potential evaporation

In WAVES, the potential evaporation was calculated by direct application of the Penman-Monteith equation.

$$\lambda E_s = \frac{\Delta R_{ns} + \rho C_p VPD_s / r_{as}}{\Delta + \gamma(1 + r_s / r_{as})} \quad (3)$$

where E_s is potential soil evaporation (mm), λ is the latent heat of vaporization (MJ kg⁻¹), Δ is the average gradient of the saturated vapor pressure versus temperature (kPa °C⁻¹), R_{ns} is the net radiation of the underlying surface (MJ m⁻² day⁻¹), ρ and C_p are the density (kg m⁻³) and the specific heat of the air at constant pressure (J kg⁻¹ K⁻¹), respectively, VPD_s is the vapor pressure deficit (kPa), γ is the psychrometric constant (kPa °C⁻¹), r_{as} is aerodynamic resistance (s m⁻¹), and r_s is soil surface resistance (s m⁻¹).

The modified WAVES added a new parameter-film cover fraction. Soil evaporation under the film cover is assumed to be zero to simulate the mulching effect. The soil evaporation under film mulching was calculated by Eq. 4,

$$E_{s_film} = (1 - f_m)E_s \quad (4)$$

where E_{s_film} is potential soil-film evaporation (mm), f_m is the film cover fraction.

Farmers try their best to keep the film mulching intact; film degradation largely occurs during late crop growth. In this study, a simplified piecewise linear process of f_m was approximated to simulate the degradation of the film. We assumed that the film was nearly complete during the early growth period, following which the degradation was linear. Visual assessments during the field trial in the 2021 experiment revealed a 40% cover fraction at the end of the growing season. Therefore, we used this value as the final film cover fraction for both experimental years. Fig. 1 depicts the film cover fraction through the whole growing season.

2.3.2. Function 2 strengthened underlying surface reflectance

The film has a larger albedo than the soil. With film mulching, the reflectivity of the underlying surface (soil-film system) is greater than that for the bare soil. A modified underlying surface reflectivity (Eq. 5) was adopted from a previous study (Ai and Yang, 2016), which was conducted at the same station. Thus, the same parameters were used in

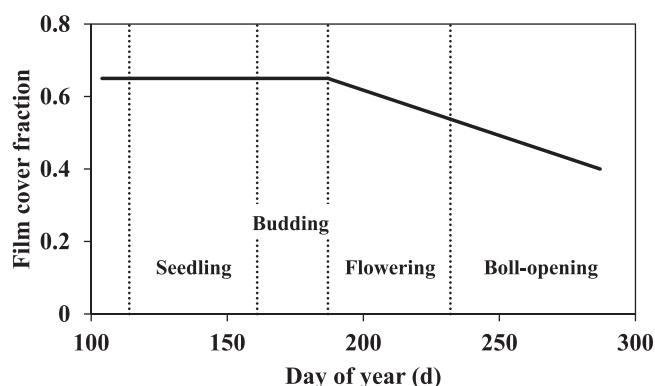


Fig. 1. Dynamic film cover fraction through the whole growing season in 2021.

the current study. In addition, the reflectivity function considered multiple reflections between mulch and canopy and the effects of solar zenith angle, LAI, and soil moisture, resulting in increased reflectance. Surface reflectance under plastic mulch was calculated as follows.

$$\alpha_{s_film} = f_m \left(r_m + \frac{\alpha_s \tau_m^2}{1 - \alpha_s r_m} \right) \exp(ah_\theta + b\theta + cLAI) + (1 - f_m)\alpha_s \quad (5)$$

where α_{s_film} is the underlying surface (soil-film system) reflectance, r_m and α_s are the reflectance of film and soil, respectively, τ_m is the transmittance of the plastic film, h_θ is the solar zenith angle (rad), θ is the soil water content ($m^3 m^{-3}$), and a, b, and c are fitted constants from Ai and Yang (2016)'s research based on experimental observations, considered as 20.42, 1.42, and 20.04, respectively, in this study.

2.3.3. Function 3 soil resistance

Film mulching prevent water escaping from soil and the soil resistance under film mulching is larger than that under bare soil. When the soil is partially mulched, the generalized soil resistance is between the resistance under film mulching and the resistance of bare soil when using the one-dimensional model. The soil resistance using the original WAVES model is calculated as follows:

$$r_s = \frac{\tau l}{p_{soil} D_m} \quad (6)$$

where p_{soil} is the porosity of the soil, D_m is the molecular diffusion coefficient for water vapor ($m^2 s^{-1}$), τ is a tortuosity factor, and l is the depth of the air-dry soil layer (m); the minimum value is the first layer. The depth of the air-dry soil layer was determined by investigating the soil water potential profile to find how deep below the surface soil is below or equal to the air-dry potential. The soil water potential was determined dynamically by solving Richards' equation. The air-dry potential was calculated from the sum of half the minimum soil water potential and half the wilting point water potential.

When running the WAVES model, the depth of the air-dry soil layer was always the first layer. The first layer was set at 0.001 m, and the soil resistance was $191 s m^{-1}$ in the original WAVES model, which was relatively small compared to Qin et al. (2018)'s research of $1280 s m^{-1}$ under mulching environment and was not suitable for mulching environments. Soil surface resistance regulates the movement of water vapors from the interior to the soil surface, and it depends strongly on the soil water content of the upper layer (θ_{soil}) (Zhao et al., 2015). Soil surface resistance is more commonly studied as a function of soil water content. In this study, the measured daily soil evaporation in the 2021 experiment was used to calculate r_s by solving Eq. 3. Three common functions were evaluated in this study: (Wang et al., 2019; Yang et al., 2020; Li et al., 2013; Zhao et al., 2015)

$$r_s = \exp(8.206 - 4.225 \theta_{soil}) \quad (7)$$

$$r_s = 250 \cdot \frac{\theta_{sat}}{\theta_{soil}} - 150 \quad (8)$$

$$r_s = 1.265 \cdot \left(\frac{\theta_{sat}}{\theta_{soil}} \right)^{5.418} \quad (9)$$

where θ_{soil} is the soil water content ($m^3 m^{-3}$), and θ_{sat} is the soil-saturated water content ($m^3 m^{-3}$). Average values of the surface 0–10 cm of soil were used.

The soil resistance was calculated according to Eq. 3.

$$r_s = \frac{\Delta R_{ns} + \frac{\rho C_p V P D_s}{r_{as}} - (\Delta + \gamma) \lambda E_s}{\gamma \lambda E_s / r_{as}} \quad (10)$$

The observed and selected relationships between r_s and θ_{soil} are shown in Fig. 2. Of the evaluated equations, Eq. 8 showed the best performance in simulating the measured data with the lowest root mean

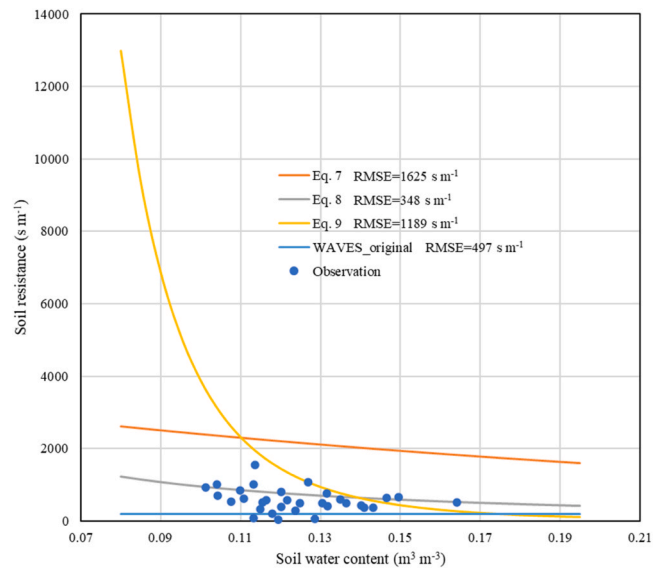


Fig. 2. Comparison of soil surface resistance responses to soil water content for three equations from published papers and the original WAVES model. RMSE is the root mean square error between different equations and observations.

square error ($348 s m^{-1}$). Eq. 8 has been validated in several crops, including cotton (Anadranistakisa et al., 2000). Because we did not have abundant data to establish a new and robust relationship, Eq. 8 was used in this study. Under irrigation, the surface resistance was set as zero.

2.4. Parameter sensitivity analysis and model calibration

The model includes three types of parameters, namely, meteorological, soil, and crop parameters. Meteorological parameters were obtained from the meteorological station at each site. Soil parameters, such as soil hydraulic properties, were measured and adjusted manually to achieve good agreement between the measured soil water content and water potential.

For the 21 crop parameters, a sensitivity analysis was first conducted using the Sobolj method (Sobolj, 2001) for both the modified and original models. Detailed sensitivity results are shown in Fig. S3. Results were similar between the two models (modified and original) and seven parameters (salt sensitivity factor, maximum production rate, optimum growth temperature, light extinction coefficient, aboveground partitioning factor, accumulated temperature requirements, and semi-optimum growth temperature) showed higher sensitivity to the model output. The accumulated temperature requirement parameter was determined using the measured data. The remaining six sensitive parameters were determined through a calibration process using the Shuffled Complex Evolution approach (SCE-UA, Duan et al., 1994). Because there were more data available from experiment A, experiment A was used for parameter calibration, whereas experiment B was used for model validation. The calibration target was set as the sum of the normalized root mean square error of the soil water content, LAI, and evaporation. The same calibration process was used for both the modified and original models. Crop parameters after calibration are shown in Table 1. The original model has a bigger value of the light extinction coefficient (0.95) than the modified value (0.71). This may be because the original model cannot take into account the film mulching effect and in order to simulate evaporation that is closer to the measured value, the original model tends to take a larger extinction coefficient value (approaching the upper bound-0.95), resulting in less energy reaching the soil surface for evaporation and then the less soil evaporation.

Table 1
Main parameters used in the WAVES model after calibration.

No.	Parameter	Value in the original model	Value in the modified model	Unit	Source
1	Albedo of the canopy	0.2	0.2	-	(Monteith and Unsworth, 2013)
2	Albedo of the soil	0.1	0.1	-	Estimated
3	Rainfall interception coefficient	0.0003	0.0003	m day ⁻¹ LAI ⁻¹	(Vertessy et al., 1996)
4	Light extinction coefficient	0.95	0.71	-	Calibrated
5	Maximum production rate	0.035	0.030	μmol m ⁻² s ⁻¹	Calibrated
6	Slope parameter for the stomatal conductance model	0.9	0.9	-	(Leuning, 1995)
7	IRM weighting of water	1.5	1.5	-	(Tian et al., 2017)
8	IRM weighting of nutrients	0.5	0.5	-	(Tian et al., 2017)
9	Ratio of stomatal to mesophyll conductance	0.2	0.2	-	(Zhang and Dawes, 1998)
10	Temperature when the growth rate is ½ of Optimum	19.05	18.74	°C	Calibrated
11	Temperature when the growth rate is optimum	31.96	28.04	°C	Calibrated
12	Degree-daylight hours of the growing season	36000	36000	°C hr	Estimated
13	Saturation light intensity	1200	1200	μmol m ⁻² day ⁻¹	(Wu et al., 1994)
14	Specific leaf area	28	28	LAI (kgC) ⁻¹	(Charles-Edwards, 1982)
15	Leaf respiration coefficient	0.0007	0.0007	kgC (kgC) ⁻¹	(Running and Coughlan, 1988)
16	Stem respiration coefficient	0.0001	0.0001	kgC (kgC) ⁻¹	(Running and Coughlan, 1988)
17	Root respiration coefficient	0.0006	0.0006	kgC (kgC) ⁻¹	(Running and Coughlan, 1988)
18	Leaf mortality rate	0.0004	0.0004	fraction of C d ⁻¹	(Running and Coughlan, 1988)
19	Aboveground partitioning factor	0.79	0.74	-	Calibrated
20	Salt sensitivity factor	0.033	0.063	-	Calibrated
21	Aerodynamic resistance	40	40	s m ⁻¹	(Brutsaert, 1982)

2.5. Statistical analysis

Statistical indices, including the root mean square error (RMSE), the normalized root mean square error (NRMSE), and the index of agreement (IoA) were used to evaluate the model. They were computed using the following equations.

$$RMSE = \sqrt{\frac{\sum_{i=1}^n (O_i - S_i)^2}{n}} \quad (11)$$

$$NRMSE = \frac{RMSE}{\bar{O}} \quad (12)$$

$$IoA = 1 - \frac{\sum_{i=1}^n (O_i - S_i)^2}{\sum_{i=1}^n (|S_i - \bar{O}| + |O_i - \bar{O}|)^2}, \quad (13)$$

where O_i and S_i are the observed and simulated values, respectively, \bar{O} is the average of observed values, and n is the number of observations.

3. Results

3.1. Performance of individual functions

All three functions affected evaporation (Fig. 3). Function 1 greatly reduced the evaporation, with average evaporation of 1.00 mm per day, whereas the original model resulted in an average evaporation of 1.65 mm. The evaporation change throughout the whole growing season was less pronounced after applying Function 1. Simulated evaporation from the original WAVES model was mostly higher than that obtained using Function 1, whereas reverse results were observed on certain days (for example days 125–131). In the flowering and boll-opening stages, we can see the small but visible differences comparing Function 1 and Function 1- in Fig. 3. The modification using dynamic film cover fraction mitigated the reduction in evaporation which increased a small amount (7.82 mm in total) compared with that obtained using a constant film cover fraction (Function 1- in Fig. 3).

Underlying surface reflectance after applying Function 2 is presented in Fig. S4. The soil albedo was 0.1. After applying Function 2, the underlying surface albedo was more than 0.1 due to the albedo contributed by film mulching (0.13), which varied from 0.12 to 0.174. The line trend depicted in Fig. S4 indicated that the surface albedo was more related to the surface soil water content. The strengthened underlying surface resistance affects the radiation transfer, thereby decreasing the net radiation caught by it (5.64%). Thus, Function 2 slightly reduced the evaporation with an average evaporation of 1.63 mm, as shown in Fig. 3.

The application of Function 3 caused the soil resistance to fluctuate between 279 and 1821 s m⁻¹, as shown in Fig. S5, and it varied with the changes in the soil water content. Function 5 greatly reduced evaporation, with an average evaporation of 1.01 mm, second only to the effect produced by Function 1. The surface resistance was set as zero during irrigation, and the water supply capacity was sufficient after irrigation, such that the evaporation on the irrigation day with the modified model was similar to that with the original model, as shown in Fig. 3.

3.2. Performance of combined functions

3.2.1. Evaporation

We simultaneously applied the three functions, and the modified and original models were calibrated using the same methods and steps. The measured and simulated soil evaporation by the original and modified models after calibration are shown in Fig. 4. The 2021 experiment generated fewer data compared to the 2010 experiment. The measured evaporation varied from 0.09 to 0.33 mm and from 0.14 to 1.46 mm in 2021 and 2010, respectively. The evaporation obtained using the modified model was more consistent with the measured evaporation than that simulated by the original model (Fig. 4). The evaporation in the seedling stage by the modified model was considerably less than that by the original model, which was close to the measured data. In all, the

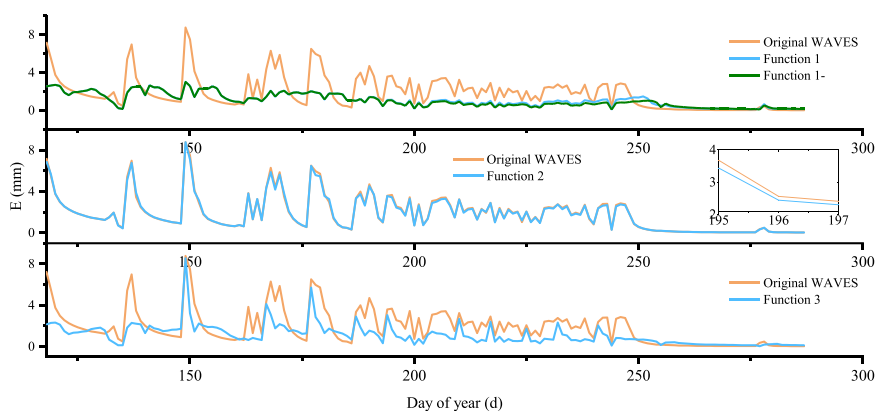


Fig. 3. Simulated evaporation through the whole growing season. Comparison of the original WAVES model with modified models by applying different functions (1, 2 and 3). Function 1- refers to simulation results obtained from Function 1, but not including the effect of the dynamic film cover fraction.

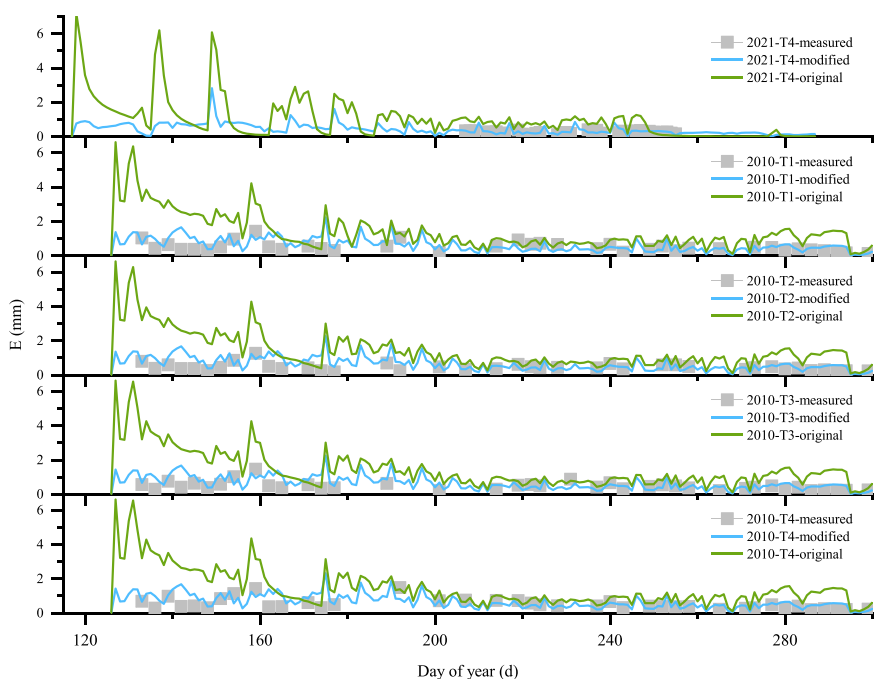


Fig. 4. Temporal variations in observed and simulated evaporations (mm) in 2021 and 2010. T1–T4 refer to different treatments, and the green and blue line imply the simulated results obtained using the original WAVES model and the modified WAVES model incorporating Functions 1, 2 and 3, respectively.

modified model produced more convincing evaporation outputs in both experiments. The RMSE of the modified model varied from 0.1 to 0.43 mm (Table 2), compared to 0.62–1.20 mm produced by the original model. In addition, the modified model resulted in better NRMSE and IoA values than the original model. The accumulated evaporation of the modified model ranged from 59 to 92 mm and 110–118 mm in 2021

and 2010, respectively. The accumulated evaporation of the original model ranged from 148 to 195 mm and 241–252 mm in 2021 and 2010, respectively. Proportions of evaporation to the total evapotranspiration (E/ET) were 14.9% and 18.4% using the modified model for the 2021 and 2010 experiments, respectively. Higher values of E/ET (32.4% and 28.3%) were found in the original model for the 2021 and 2010

Table 2
Values of evaluation indicators of simulated evaporation in 2010 and 2021.

Year	Treatment	Modified WAVES			Original WAVES		
		RMSE	NRMSE	IoA	RMSE	NRMSE	IoA
2021 (Calibration)	2021T4	0.10	0.46	0.55	0.62	2.90	0.16
2010 (Validation)	2010T1	0.43	0.83	0.36	1.13	2.21	0.31
	2010T2	0.41	0.92	0.35	1.19	2.64	0.26
	2010T3	0.41	0.87	0.41	1.20	2.57	0.28
	2010T4	0.43	0.83	0.47	1.16	2.27	0.34

Note: RMSE is the root mean square error (mm), NRMSE is the normalized root mean square error, and IoA is the index of agreement. T1–T4 refer to different treatments.

experiments, respectively.

3.2.2. Soil water content

Goodness-of-fit test indices of average soil water content in 2021 (calibration) and 2010 (validation) are shown in Table 3. The modified model produced better results in all treatments in 2 years than the original WAVES model. For instance, the index of IoA varied from 0.48 to 0.86 in the modified model, whereas it ranged from 0.30 to 0.68 in the original model. Similarly, compared with the original model, NRMSEs of soil water content under different irrigation treatments for two seasons decreased by 6.43–32.88% using the modified model. The average IoA values were 0.70 and 0.46 for the modified and original models, respectively. Fig. 5 shows the simulated and measured soil water content during the growing season. The simulated value varied largely following irrigation events. The modified model provided better agreement with the measurement than the original model. A large difference between the modified and original models, especially with time after germination, was observed. The application of the original model resulted in smaller soil water content than the modified model, because of higher evaporation at the budding stage.

3.2.3. Soil salt content

Table 4 and Fig. 6 show how the modified and original model simulate the average soil salt content. The average RMSE values for soil salt content were 1.01 g kg⁻¹ and 1.90 g kg⁻¹ for modified and original models, respectively. Overall, the modified model produced better or equal NRMSE compared with the original model. The modified model had larger IoA values, except for 2021T4. The dynamic change of the soil salt content using the modified model was more similar to the observations (Fig. 6). The original model overestimated the soil salt content in most cases, especially in the later stage. The simulated salt content gradually increased within the growing period except for 2021T4, 2010T3, and 2010T4. In these three treatments, the shape of the simulated salt content was S-shaped. The salt content increased at first and then showed a decreasing trend and approached its minimum value around the final irrigation time. After that, the salt content increased again without any more applied irrigation. Across the whole growing season, with the increase in the total irrigation amount (from T1 to T4), the salt content in the root zone displayed signs of salt washing when irrigation amount was greater than 480 mm.

3.2.4. LAI and lint yield

Fig. 7 shows temporal variations in simulated LAI and measured values. LAI was only measured in 2021. In 2021T1 and 2021T2, no large difference was recorded between the modified and original models, whereas the modified model generated noticeably better results than the original model in 2021T3 and 2021T4. Across all treatments, the average RMSE values were 0.37 and 0.59 m² m⁻² for modified and original models, respectively. The modified model reduced the NRMSE by 9.43% on average.

The results for cotton lint yield are shown in Fig. 8. The simulated

and measured data from the modified model displayed a closer relationship to the 1:1 line. The mean RMSE of the modified model was 248 kg ha⁻¹, the NRMSE was 9.46%, and the IoA was 0.93. The modified model performed well, simulating yield under different irrigation amounts and different salt environments. The original model generated a large bias in validation (an RMSE of 1615 kg ha⁻¹), indicating its poor yield reproducibility.

4. Discussion

4.1. Strengths and limitations of added functions

Function 1, which is the most widely used method to study the mulching effect, was used to introduce film cover fraction into the model. It has been reported to work efficiently (Li et al., 2019; Shen et al., 2021), and it works well in this study. Function 1 reduces the simulated evaporation and makes it closer to the actual value. In most cases, the evaporation simulated by Function 1 is smaller than that from the original model. The reason for the opposite situation (for example days 125–131) to occur is because water consumption of the modified model in the early stage (days before 125) is smaller, with more volume of water remaining on the surface and the evaporation is larger than the original model in days 125–131. Besides, there is one aspect that requires further attention. Function 1 works well when the evaporation is dominated by atmospheric evaporation capacity, which is calculated from potential evaporation (Eq. 3). Function 1 has no correction effect when the soil is very dry and the evaporation is decided by soil water supply capacity calculated from Darcy theory, not the potential evaporation calculated from Eq. 3. In most cases, Function 1 worked well and exerted the highest modification effect on soil evaporation. The film cover fraction value is based on actual management practice. Because Function 1 has a great impact on evaporation, it should be cautious to decide its value based on the field management. The uncertainty of film cover fraction will affect the uncertainty of the model parameters. The dynamic film cover fraction (Fig. 1) also contributes to water movement, increasing the practicality of the introduced factor of film cover fraction. Biodegradable mulching is becoming more commonly used as an alternative to polyethylene mulching, and thus being able to model the dynamics of degradation in crop model applications is important. Griffin-LaHue et al. (2022) demonstrated that thermal time is a crucial factor that decides mulch degradation and established a zeroth-order kinetics model predicting the degradation rate of mulch. More process-based functions should be studied in the future.

Function 2 exerted a small impact because of the limited change it could produce in soil reflectivity. Compared to the original model, the radiation reduced 5.64% due to the increased surface albedo, and the evaporation reduced 1.38%. The rate of reduction in evaporation was lower than that of radiation because evaporation is affected both by radiation and aerodynamics. Eq. 2 influences the distribution of radiation by altering reflectivity. It is worth noting that the changes in reflectivity not only affect the radiation reaching the surface for

Table 3

Values of evaluation indicators of simulated soil water content in 2021 and 2010.

Year	Treatment	Modified WAVES			Original WAVES		
		RMSE	NRMSE	IoA	RMSE	NRMSE	IoA
2021 (Calibration)	2021T1	0.03	0.21	0.72	0.06	0.50	0.41
	2021T2	0.01	0.18	0.83	0.02	0.25	0.68
	2021T3	0.04	0.28	0.66	0.07	0.47	0.50
	2021T4	0.02	0.14	0.86	0.08	0.47	0.48
2010 (Validation)	2010T1	0.02	0.08	0.48	0.05	0.18	0.30
	2010T2	0.02	0.07	0.56	0.05	0.15	0.40
	2010T3	0.01	0.05	0.72	0.04	0.12	0.41
	2010T4	0.02	0.05	0.77	0.04	0.11	0.53

Note: RMSE is the root mean square error (cm³ cm⁻³), NRMSE is the normalized root mean square error, and IoA is the index of agreement. T1–T4 refer to different treatments.

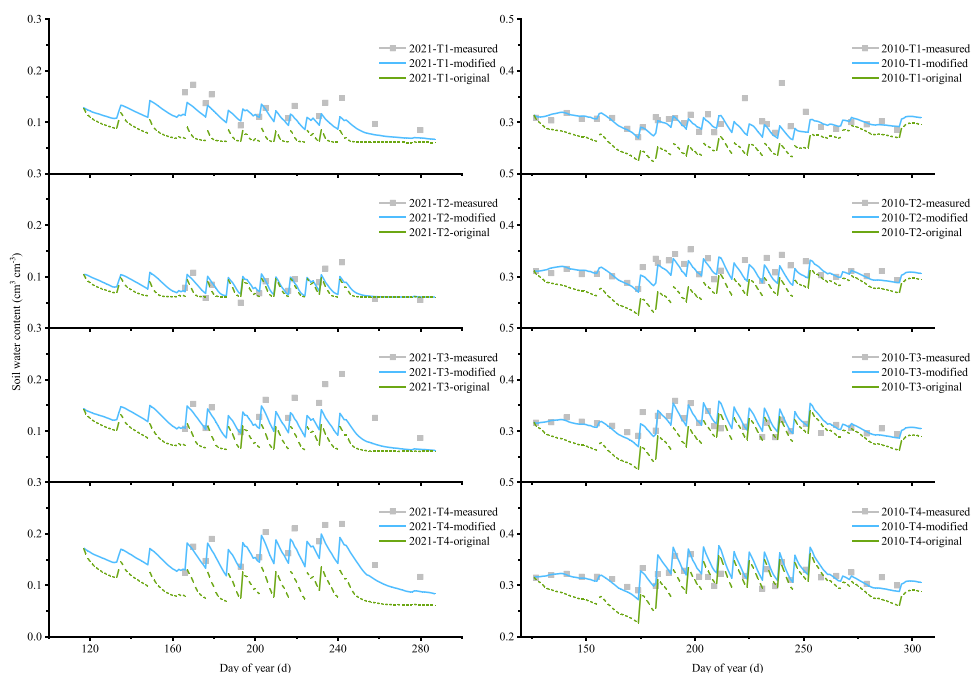


Fig. 5. Temporal variations in observed and simulated average soil water contents of 0–80 cm depth in 2021 and 2010. T1–T4 refer to different treatments, and the green and blue line imply the simulated results obtained using the original WAVES model and the modified WAVES model incorporating Functions 1, 2 and 3, respectively.

Table 4
Values of evaluation indicators of simulated soil salt content in 2021 and 2010.

Year	Treatment	Modified WAVES			Original WAVES		
		RMSE	NRMSE	IoA	RMSE	NRMSE	IoA
2021 (Calibration)	2021T1	1.69	0.19	0.43	3.06	0.34	0.43
	2021T2	1.63	0.60	0.14	1.63	0.60	0.06
	2021T3	0.48	0.22	0.77	0.73	0.34	0.65
	2021T4	0.70	0.23	0.28	1.11	0.37	0.37
2010 (Validation)	2010T1	0.67	0.10	0.74	1.52	0.23	0.54
	2010T2	0.79	0.12	0.56	1.70	0.25	0.46
	2010T3	0.90	0.12	0.57	2.24	0.30	0.35
	2010T4	1.22	0.16	0.58	3.19	0.41	0.26

Note: RMSE is the root mean square error (g kg^{-1}), NRMSE is the normalized root mean square error, and IoA is the index of agreement. T1–T4 refer to different treatments.

evaporation but also influence the radiation received by plants for transpiration. The introduction of Eq. 2 in the WAVES model allows for the consideration of the impact of film mulching on transpiration through changes in reflectivity.

Function 3 changed the soil resistance, causing a drastic reduction in evaporation. This finding indicated that soil resistance is an important variable. The method that the original WAVES used to characterize surface resistance under film mulching condition is unsuitable. Because the depth of the air-dry soil layer is now always the first layer in the original model, how to determine the air-dry potential and get the depth of the air-dry soil layer could be further studied in the future. In the modified model, soil resistance was slightly overestimated (Fig. 2). Texture and depth selected to measure the soil water content varied among different studies (Zhao et al., 2015), possibly resulting in variable relationships between r_s and θ_{soil} . Function 3, taken from another study, was directly used in this study and therefore, we believe, resulted in overestimation. Relationships between r_s and θ_{soil} could be specified once data are available.

Function 2 and 3 calculate the actual potential evaporation capacity under a film mulching condition. Function 1 assumes that the film mulching area does not evaporate, and then calculates a one-dimensional comprehensive evaporation. Although certain

modifications exerted limited impact, they provided a better mechanism to simulate crops under film mulching. Altogether, the results showed that the incorporation of these formulas into the original model is highly effective.

4.2. Evaluation of modified model under film mulching conditions

A daily process-based hydrological crop model WAVES was modified using three functions related to mulching effects. All three functions contributed to improved outcomes; Function 1 exerted the biggest modification effects on soil water status, followed by Function 3. The modified model generated results on evaporation, soil water content, soil salt content, LAI, and yield with higher accuracy than the original model, decreasing NRMSE by 173%, 15%, 14%, 9%, and 35%, respectively. In all, the evaporation performance was greatly improved. Moreover, the model produced a more realistic E/ET (less than 20%) under film mulching conditions, and the value was similar to that reported by Tian et al. (2016). Soil water content greatly improved after modification, with different contributions in different growing stages. In the seedling stage, when the film mulching exerted the highest effects on the system, the modified model considerably better estimated the soil-water dynamics than the original model, which has also been

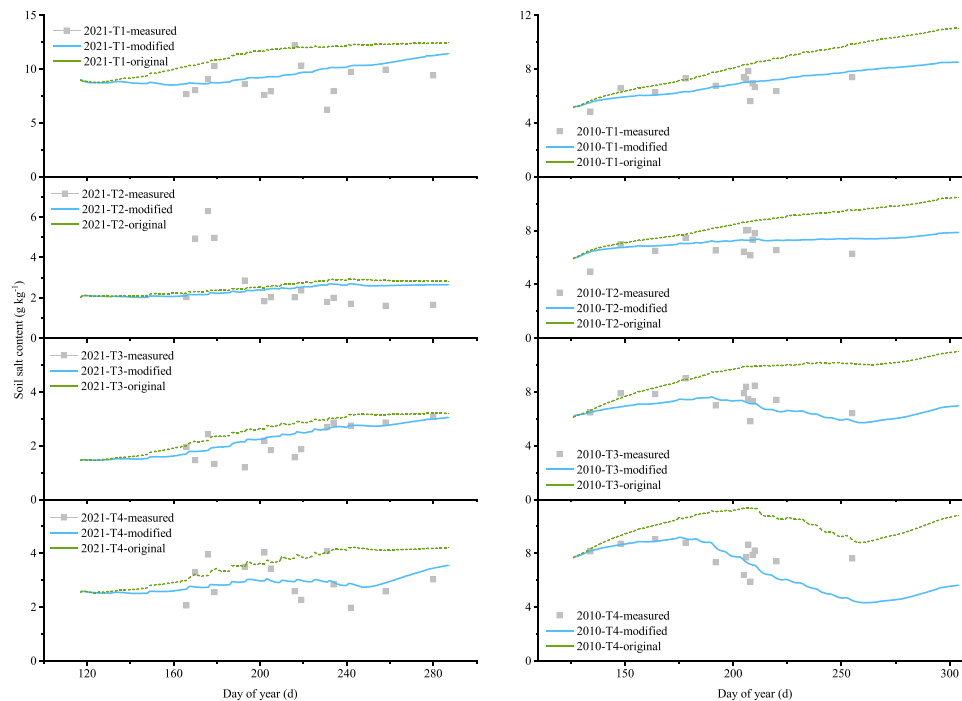


Fig. 6. Temporal variations in observed and simulated average soil salt contents of 0–80 cm depth in 2021 and 2010. T1–T4 refer to different treatments, and the green and blue line imply the simulated results obtained using the original WAVES model and the modified WAVES model incorporating Functions 1, 2 and 3, respectively.

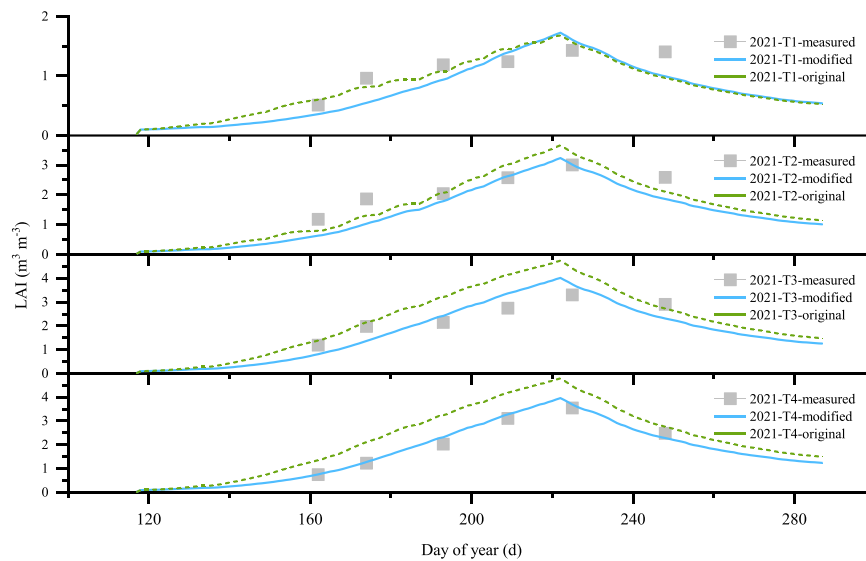


Fig. 7. Temporal variations in observed and simulated LAI values in 2021. T1–T4 refer to different treatments, and the green and blue line imply the simulated results obtained using the original WAVES model and the modified WAVES model incorporating Functions 1, 2 and 3, respectively.

reported by Zhao et al. (2020) who modified the SWAP model to take into account the mulching effect.

Because the simulated salt moves with water, the soil salt content is also affected by mulching. There were three soil salt content measurements for 2021T2 that had abnormally large values that deviated from other points. The measured data could have been affected by the sampling location and soil heterogeneity, thus leading to a larger error. Regarding the simulation of soil salt content, the salinity simulated by the original model was higher than that by the modified model, which could be attributed to the stronger evaporation capacity of the original model, resulting in greater traction of water moving toward the surface. The salt movement within the water resulted in increased salt

accumulation of the original model in the root zone. Throughout the entire growth period, the soil salt content mainly shown increasing trend except for the case with larger irrigation amount. The simulated average salt content showed a decreasing trend with similar irrigation amounts in different years, that is, 480 mm (T4) in 2021 and 487.5 mm (T3) in 2010. When the irrigation amount was 600 mm (T4) in 2010, the final salt storage (5.62 g kg^{-1}) was significantly less than the initial amount (7.66 g kg^{-1}), and the salt washing percentage was 26.63%. Tan et al. (2018) performed a similar study on cotton in southern Xinjiang, China, and demonstrated that the treatment with an irrigation amount of over 412.5 mm led to a decreasing trend in average soil salt, which is consistent with the findings of our study. Another study (Xu et al., 2019)

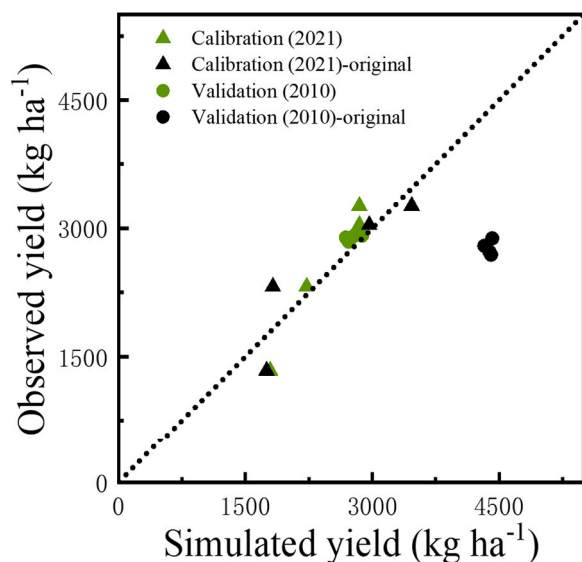


Fig. 8. Relationship between observed cotton lint yield and simulated yield. The green points reflect the results of the modified model, whereas the black points correspond to the results of the original model. The triangle and circle represent calibration and verification results, respectively.

conducted in northwest China reported higher soil desalting efficiency when the irrigation amount was in the range of 400–600 mm. When considering washing salt with abundant water, it is necessary to balance the relationship between water saving and salt washing efficiency.

The modified model efficiently simulated LAI. However, there is a lack of validation for simulated LAI results related to crop growth indicators. LAI data is needed for further validation in the future study. The modified model could efficiently forecast yield with high accuracy both during calibration and validation. Yield is obtained by multiplying biomass by harvest index and biomass is highly correlated with LAI. The good performance of yield could indirectly demonstrate the rationality of leaf area index simulation at current research. During validation, the original model simulated a larger yield than the measured value, which could be related to its strong evaporation effect. This component of evaporation does not contribute to plant yield. However, the yield formation in the WAVES model is proportional to the ratio of actual ET and potential ET. Thus, the overestimated evaporation was also included, resulting in overestimated yield.

This model concentrated on film mulching effects on soil water movement and its indirect effects on crop growth. In addition, the film mulch could trap outgoing terrestrial radiation, thereby increasing above- and below-ground temperatures (Lisson et al., 2016), which is not included in our model. The specific results are affected by the calibrated data. The crop varieties in the two field experiments were different and we lacked the validation of LAI, which would affect the uncertainty of the parameters but it didn't affect our conclusion in this paper. Based on the same calibration method, we infer that the modified model has better mechanisms and performance than the original model to simulate crops under film mulching. More experiments on different areas and different crops are warranted to enhance the robustness and reliability in the future. Although the modified WAVES model cannot be immediately used by farmers, researchers or policymakers are encouraged to try and design scenarios to improve the situation of water scarcity.

5. Conclusions

A modified WAVES model incorporating the film mulching effect was analyzed in southern Xinjiang, China. Three functions working on potential evaporation, underlying surface albedo, and soil resistance

were introduced into the original WAVES model. Calibration and validation were performed using 2 years of data obtained from cotton field experiments in areas with severe drought and serious salinization. The function modifying potential evaporation provided the greatest effect, followed by the modification on soil resistance. The application of dynamic film cover fraction and strengthened underlying surface reflectance exerted smaller effects, while they provided a better mechanism to simulate crops under film mulching. Altogether, the modified model better estimated evaporation, soil water content, soil salt content, LAI, and yield than the original model indicating that the modified WAVES model could be valuable in field management under film mulching. Note that the modified WAVES model was calibrated based on our experiment data, further calibration and validation should be conducted once data is available to improve the parameters' robustly and applicability.

Declaration of Competing Interest

The authors declare that they have no known competing financial interests or personal relationships that could have appeared to influence the work reported in this paper.

Data availability

Data will be made available on request.

Acknowledgments

This study was financially supported by the National Key R&D Program of China (No. 2022YFD1900503). We are grateful to the China Scholarship Council for supporting Ms. Qihua Yu 10 months stay at the Swedish University of Agricultural Sciences.

Appendix A. Supporting information

Supplementary data associated with this article can be found in the online version at [doi:10.1016/j.agwat.2023.108470](https://doi.org/10.1016/j.agwat.2023.108470).

References

- Ai, Z., Yang, Y., 2016. Modification and validation of priestley-taylor model for estimating cotton evapotranspiration under plastic mulch condition. *J. Hydrometeorol.* 17, 1281–1293.
- Anadranistakisa, M., Liakatasb, A., Kerkidesb, P., Rizosb, S., Gavanosib, J., Poulouvasiliab, A., 2000. Crop water requirements model tested for crops grown in Greece. *Agric. Water Manag.* 45, 297–316.
- Barron, O.V., Crosbie, R.S., Dawes, W.R., Charles, S.P., Pickett, T., Donn, M.J., 2012. Climatic controls on diffuse groundwater recharge across Australia. *Hydrol. Earth Syst. Sci.* 16, 4557–4570.
- Brutsaert, W., 1982. *Evaporation into the atmosphere: theory, history, and applications*. Kluwer Academic Publisher, Dordrecht, The Netherlands.
- Caparas, M., Zobel, Z., Castanho, A.D.A., Schwalm, C.R., 2021. Increasing risks of crop failure and water scarcity in global breadbaskets by 2030. *Environ. Res. Lett.* 16.
- Charles-Edwards, D.A., 1982. *Physiological determinants of crop growth*. Academic Press, New South Wales.
- Cheng, L., Zhang, L., Wang, Y.-P., Yu, Q., Eamus, D., 2014. Quantifying the effects of elevated CO₂ on water budgets by combining FACE data with an ecohydrological model. *Ecohydrology* 7, 1574–1588.
- Crosbie, R.S., Scanlon, B.R., Mpelasoka, F.S., Reedy, R.C., Gates, J.B., Zhang, L., 2013. Potential climate change effects on groundwater recharge in the High Plains Aquifer, USA. *Water Resour. Res.* 49, 3936–3951.
- Ding, R., Kang, S., Zhang, Y., Hao, X., Tong, L., Li, S., 2015. A dynamic surface conductance to predict crop water use from partial to full canopy cover. *Agric. Water Manag.* 150, 1–8.
- Duan, Q., Sorooshian, S., Gupta, V.K., 1994. Optimal use of the SCE-UA global optimization method for calibrating watershed models. *J. Hydrol.* 158, 265–284.
- Elliott, J., Deryng, D., Müller, C., Frieler, K., Konzmann, M., Gerten, D., Glotter, M., Flörke, M., Wada, Y., Best, N., Eisner, S., Fekete, B.M., Folberth, C., Foster, I., Gosling, S.N., Haddeland, I., Khabarov, N., Ludwig, F., Masaki, Y., Olin, S., Rosenzweig, C., Ruane, A.C., Satoh, Y., Schmid, E., Stacke, T., Tang, Q., Wisser, D., 2014. Constraints and potentials of future irrigation water availability on agricultural production under climate change. *Proc. Natl. Acad. Sci. U. S. A.* 111, 3239–3244.

- Gao, F., Huang, Q., Sun, X., Yan, Z., 2011. Study on dynamic changes of the soil salinization in the upper stream of the Tarim River based on RS and GIS. *Procedia Environ. Sci.* 11, 1135–1141.
- Gao, H., Yan, C., Liu, Q., Ding, W., Chen, B., Li, Z., 2019. Effects of plastic mulching and plastic residue on agricultural production: a meta-analysis. *Sci. Total Environ.* 651, 484–492.
- Gharun, M., Possell, M., Vervoort, R.W., Adams, M.A., Bell, T.L., 2018. Can a growth model be used to describe forest carbon and water balance after fuel reduction burning in temperate forests? *Sci. Total Environ.* 615, 1000–1009.
- Griffin-LaHue, D., Ghimire, S., Yu, Y., Scheenstra, E.J., Miles, C.A., Flury, M., 2022. In-field degradation of soil-biodegradable plastic mulch films in a Mediterranean climate. *Sci. Total Environ.* 806, 150238.
- Han, J., Jia, Z., Wu, W., Li, C., Han, Q., Zhang, J., 2014. Modeling impacts of film mulching on rainfed crop yield in Northern China with DNDC. *Field Crops Res* 155, 202–212.
- He, Q., Li, S., Kang, S., Yang, H., Qin, S., 2018. Simulation of water balance in a maize field under film-mulching drip irrigation. *Agric. Water Manag.* 210, 252–260.
- Hou, P., Cui, Z., Bu, L., Yang, H., Zhang, F., Li, S., 2014. Evaluation of a modified Hybrid-Maize model incorporating a newly developed module of plastic film mulching. *Crop Sci.* 54, 2796–2804.
- Hu, S., Shen, Y., Chen, X., Gan, Y., Wang, X., 2013. Effects of saline water drip irrigation on soil salinity and cotton growth in an Oasis Field. *Ecohydrology* 6, 1021–1030.
- Kader, M.A., Senge, M., Mojid, M.A., Ito, K., 2017. Recent advances in mulching materials and methods for modifying soil environment. *Soil Tillage Res* 168, 155–166.
- Kang, S., Zhang, L., Liang, Y., Dawes, W., 2003. Simulation of winter wheat yield and water use efficiency in the Loess Plateau of China using WAVES. *Agric. Syst.* 78, 355–367.
- Kang, S., Hao, X., Du, T., Tong, L., Su, X., Lu, H., Li, X., Huo, Z., Li, S., Ding, R., 2017. Improving agricultural water productivity to ensure food security in China under changing environment: From research to practice. *Agric. Water Manag.* 179, 5–17.
- Kim, Y., Berger, S., Kettering, J., Tenhunen, J., Haas, E., Kiese, R., 2014. Simulation of N₂O emissions and nitrate leaching from plastic mulch radish cultivation with LandscapeDNDC. *Ecol. Res.* 29, 441–454.
- Leuning, R., 1995. A critical appraisal of a combined stomatal-photosynthesis model for C₃ plants. *Plant Cell Environ.* 18, 339–355.
- Li, M., Du, Y., Zhang, F., Bai, Y., Fan, J., Zhang, J., Chen, S., 2019. Simulation of cotton growth and soil water content under film-mulched drip irrigation using modified CSM-CROPGRO-cotton model. *Agric. Water Manag.* 218, 124–138.
- Li, S., Kang, S., Zhang, L., Ortega-Farías, S., Li, F., Du, T., Tong, L., Wang, S., Ingman, M., Guo, W., 2013. Measuring and modeling maize evapotranspiration under plastic film-mulching condition. *J. Hydrol.* 503, 153–168.
- Liang, H., Hu, K., Qin, W., Zuo, Q., Zhang, Y., 2017. Modelling the effect of mulching on soil heat transfer, water movement and crop growth for ground cover rice production system. *Field Crops Res* 201, 97–107.
- Lisson, S.N., Tarbath, M., Corkrey, R., Pinkard, E.A., Laycock, B., Howden, S.M., Botwright Acuña, T., Makin, A., 2016. Ambient climate and soil effects on the headspace under clear mulch film. *Agric. Syst.* 142, 41–50.
- Lv, S., Li, J., Yang, Z., Yang, T., Li, H., Wang, X., Peng, Y., Zhou, C., Wang, L., Abdo, A.I., 2023. The field mulching could improve sustainability of spring maize production on the Loess Plateau. *Agric. Water Manag.* 279.
- Monteith, J.L., Unsworth, M.H., 2013. Principles of environmental physics, 4th ed... Academic Press, Poland, p. 82.
- Qin, S., Li, S., Yang, K., Hu, K., 2018. Can plastic mulch save water at night in irrigated croplands? In: *J. Hydrol.* 564, pp. 667–681.
- Qureshi, A.S., Ahmad, W., Ahmad, A.-F.A., 2013. Optimum groundwater table depth and irrigation schedules for controlling soil salinity in central Iraq. *Irrig. Drain.* 62, 414–424.
- Running, S.W., Coughlan, J.C., 1988. A general model of forest ecosystem processes for regional applications I. Hydrologic balance, canopy gas exchange and primary production processes. *Ecol. Modell.* 42, 125–154.
- Saglam, M., Sintim, H.Y., Bary, A.I., Miles, C.A., Ghimire, S., Inglis, D.A., Flury, M., 2017. Modeling the effect of biodegradable paper and plastic mulch on soil moisture dynamics. *Agric. Water Manag.* 193, 240–250.
- Shen, H., Gao, Y., Guo, F., Wang, Y., Ma, X., 2021. A modified DSSAT-CERES model for simulating summer maize growth under film mulching. *Agron. J.* 113, 4819–4831.
- Shukla, S., Shrestha, N.K., Jaber, F.H., Srivastava, S., Obreza, T.A., Boman, B.J., 2014. Evapotranspiration and crop coefficient for watermelon grown under plastic mulched conditions in sub-tropical Florida. *Agric. Water Manag.* 132, 1–9.
- Silberstein, R.P., Dawes, W.R., Bastow, T.P., Byrne, J., Smart, N.F., 2013. Evaluation of changes in post-fire recharge under native woodland using hydrological measurements, modelling and remote sensing. *J. Hydrol.* 489, 1–15.
- Sintim, H.Y., Bary, A.I., Hayes, D.G., Wadsworth, L.C., Anunciado, M.B., English, M.E., Bandopadhyay, S., Schaeffer, S.M., DeBruyn, J.M., Miles, C.A., Reganold, J.P., Flury, M., 2020. In situ degradation of biodegradable plastic mulch films in compost and agricultural soils. *Sci. Total Environ.* 727, 138668.
- Sobol, I.M., 2001. Global sensitivity indices for nonlinear mathematical models and their Monte Carlo estimates. *Math. Comput. Simul.* 55, 271–280.
- Steinmetz, Z., Wollmann, C., Schaefer, M., Buchmann, C., David, J., Troger, J., Munoz, K., Fror, O., Schaumann, G.E., 2016. Plastic mulching in agriculture. Trading short-term agronomic benefits for long-term soil degradation? *Sci. Total Environ.* 550, 690–705.
- Su, N., Bethune, M., Mann, L., Heuperman, A., 2005. Simulating water and salt movement in tile-drained fields irrigated with saline water under a Serial Biological Concentration management scenario. *Agric. Water Manag.* 78, 165–180.
- Sun, Q., Wang, Y., Chen, G., Yang, H., Du, T., 2018. Water use efficiency was improved at leaf and yield levels of tomato plants by continuous irrigation using semipermeable membrane. *Agric. Water Manag.* 203, 430–437.
- Tan, S., Wang, Q., Zhang, J., Chen, Y., Shan, Y., Xu, D., 2018. Performance of AquaCrop model for cotton growth simulation under film-mulched drip irrigation in southern Xinjiang, China. *Agric. Water Manag.* 196, 99–113.
- Tian, F., Yang, P., Hu, H., Dai, C., 2016. Partitioning of cotton field evapotranspiration under mulched drip irrigation based on a dual crop coefficient model. *Water* 8, 72.
- Tian, F., Feng, X., Zhang, L., Fu, B., Wang, S., Lv, Y., Wang, P., 2017. Effects of revegetation on soil moisture under different precipitation gradients in the Loess Plateau, China. *Hydrol. Res.* 48, 1378–1390.
- Vertessy, R.A., Hatton, T.J., Benyon, R.G., Dawes, W.R., 1996. Long-term growth and water balance predictions for a mountain ash (*Eucalyptus regnans*) forest catchment subject to clear-felling and regeneration. *Tree Physiol.* 16, 221–232.
- Wang, H., Zhang, L., Dawes, W.R., Liu, C., 2001. Improving water use efficiency of irrigated crops in the North China Plain—measurements and modelling. *Agric. Water Manag.* 48, 151–167.
- Wang, P., Deng, Y., Li, X.-Y., Wei, Z., Hu, X., Tian, F., Wu, X., Huang, Y., Ma, Y.-J., Zhang, C., Wang, Y., Li, E., Wang, J., 2019. Dynamical effects of plastic mulch on evapotranspiration partitioning in a mulched agriculture ecosystem: Measurement with numerical modeling. *Agric. Meteorol.* 268, 98–108.
- Wu, H., Jr, E.J.R., Hatton, T., Walker, J., 1994. An integrated rate methodology (IRM) for multi-factor growth rate modelling. *Ecol. Eng.* 73, 97–116.
- Xu, C., Tian, J., Wang, G., Nie, J., Zhang, H., 2019. Dynamic simulation of soil salt transport in arid irrigation areas under the HYDRUS-2D-based rotation irrigation mode. *Water Resour. Manag.* 33, 3499–3512.
- Xu, Z., Wallach, R., Song, J., Mao, X., 2023. Effect of plastic film colours and perforations on energy distribution, soil temperature, and evaporation. *Agronomy* 13.
- Yang, D., Li, S., Kang, S., Du, T., Guo, P., Mao, X., Tong, L., Hao, X., Ding, R., Niu, J., 2020. Effect of drip irrigation on wheat evapotranspiration, soil evaporation and transpiration in Northwest China. *Agric. Water Manag.* 232, 106001.
- Yang, Q., Zuo, H., Xiao, X., Wang, S., Chen, B., Chen, J., 2012. Modelling the effects of plastic mulch on water, heat and CO₂ fluxes over cropland in an arid region. *J. Hydrol.* 452–453, 102–118.
- Yu, Q., Kang, S., Hu, S., Zhang, L., Zhang, X., 2021. Modeling soil water-salt dynamics and crop response under severely saline condition using WAVES: Searching for a target irrigation volume for saline water irrigation. *Agric. Water Manag.* 256.
- Zhang, L., Dawes, W.R., 1998. WAVES: an integrated energy and water balance model, first ed... CSIRO Land and Water, Canberra.
- Zhao, P., Li, S., Li, F., Du, T., Tong, L., Kang, S., 2015. Comparison of dual crop coefficient method and Shuttleworth-Wallace model in evapotranspiration partitioning in a vineyard of northwest China. *Agric. Water Manag.* 160, 41–56.
- Zhao, Y., Mao, X., Shukla, M.K., 2020. A modified SWAP model for soil water and heat dynamics and seed-maize growth under film mulching. *Agric. Meteorol.* 292–293, 108127.